Heliyon 9 (2023) e18503

Contents lists available at ScienceDirect

Heliyon

journal homepage: www.cell.com/heliyon

Prediction of prognosis and immunotherapy response in lung adenocarcinoma based on CD79A, DKK1 and VEGFC

Qilong Zhang [a], Mingyuan Zhao [b], Shuangyan Lin [b], Qi Han [a], He Ye [a], Fang Peng [b,**], Li Li [a,*]

[a] Department of Pharmacy, Zhejiang Hospital, Hangzhou, Zhejiang 310007, China
[b] Department of Pathology, Zhejiang Hospital, Hangzhou, Zhejiang 310007, China

ARTICLE INFO

Keywords:
Lung adenocarcinoma
Tumor immune microenvironment
Prognosis
CD79A
DKK1
VEGFC

ABSTRACT

Background: Tumor immune microenvironment (TIME) is crucial for tumor initiation, progression, and metastasis; however, its relationship with lung adenocarcinoma (LUAD) is unknown. Traditional predictive models screen for biomarkers that are too general and infrequently associated with immune genes.

Methods: RNA sequencing data of LUAD patients and immune-related gene sets were retrieved from public databases. Using the common genes shared by The Cancer Genome Atlas (TCGA) and Immunology Database and Analysis Portal (ImmPort), differential gene expression analysis, survival analysis, Lasso regression analysis, and univariate and multivariate Cox regression analyses were performed to generate a novel risk score model. LUAD cohort in International Cancer Genome Consortium (ICGC), GSE68465 cohort in Gene Expression Omnibus (GEO) and an immunohistochemical assay were used to validate the key genes constructed risk score. The LUAD-related prognosis, clinical indicators, immune infiltrate characteristics, response to immunotherapy, and response to chemotherapeutic agents in different risk groups were evaluated by CIBERSORT, ImmuCellAI, pRRophetic and other tools.

Results: The risk score model was constructed using CD79a molecule (CD79A), Dickkopf WNT signaling pathway inhibitor 1 (DKK1), and vascular endothelial growth factor C (VEGFC). High risk score was identified as a negative predictor for overall survival (OS) in subgroup analyses with tumor stage, TNM classification, therapy outcome, and ESTIMATE scores ($P < 0.05$). Low risk score was positively associated with plasma cells, memory B cells, CD8 T cells, regulatory T cells and γδT cells ($P < 0.05$). In low-risk group, programmed cell death 1 receptor (PD1), cytotoxic T-lymphocyte associated protein 4 (CTLA4), and lymphocyte activating 3 (LAG3) and indoleamine 2,3-dioxygenase (IDO) were more robustly expressed ($P < 0.05$). The treatment responses of immune checkpoint blockade (ICB) therapy and chemotherapy were likewise superior in low-risk group ($P < 0.05$). In immunohistochemical analysis, the tumor group had significantly higher levels of CD79A, DKK1, and VEGFC than the adjacent normal group ($P < 0.01$).

Conclusions: CD79A, DKK1 and VEGFC are important differential genes related to LUAD, risk score could reliably predict prognosis, composition of TIME and immunotherapy responses in

* Corresponding author. Department of Pharmacy, Zhejiang Hospital, 1229 Gudun Road, Hangzhou, Zhejiang 310007, China.
** Corresponding author. Department of Pathology, Zhejiang Hospital, 1229 Gudun Road, Hangzhou, Zhejiang 310007, China.
E-mail addresses: pengfang999@139.com (F. Peng), zjyylili@163.com (L. Li).

https://doi.org/10.1016/j.heliyon.2023.e18503
Received 15 November 2022; Received in revised form 14 July 2023; Accepted 19 July 2023
Available online 20 July 2023

LUAD patients. The excellent performance of the risk model shows its strong and broad application potential.

1. Introduction

Lung cancer is one of the cancers with the highest fatality and incidence rates worldwide. Lung adenocarcinoma (LUAD) has become the most prevalent clinical histological subtype of lung cancer in non-small cell lung cancer (NSCLC) [1,2]. The availability of imaging equipments and the use of surgery, radiotherapy, or chemotherapy, enables diagnosis and timely treatment of patients with lung cancer, resulting in significant improvement in postoperative survival. However, it is difficult to obtain good prognosis for some patients with lung cancer due to high recurrence and metastatic nature of the tumor, which limits the treatment efficacy [3]. In recent years, it has been demonstrated that some approved drugs based on gene targeting of epidermal growth factor receptor (EGFR), anaplastic lymphoma kinase (ALK), ROS Proto-oncogene 1 (ROS1), cellular-mesenchymal epithelial transition factor (c-Met) and drugs antagonizing immune checkpoint molecules, such as gefitinib and bevacizumab, can improve the survival of lung cancer patients [4]. However, there is still a subset of lung cancer patients whose driver genes for LUAD are not clear and who have not shown improvement from the use of these gene targeted drugs. Traditional significance prediction models screen for biomarkers that are too broad to be associated with immune genes [5]. Consequently, it is of great interest to search for novel LUAD biomarkers that can be used to predict patient survival and immunotherapy response in continuously updated public gene expression profiles.

The continuous crosstalk between immune cell infiltration and immune-associated genes in the tumor immune microenvironment (TIME) may provide clues for predicting the survival outcomes and immunotherapy responses of LUAD patients [6,7]. It has been shown that the types and levels of immune cells in the TIME can inhibit or promote tumor development [8]. TIME is an environment where tumors reside and is composed of various immune cells, stromal cells, cytokines, and extracellular matrix molecules [9]. The TIME of LUAD is infiltrated with numerous immune cells, such as T lymphocytes, B cells, dendritic cells (DC), macrophages, natural killer (NK) cells, etc. Emerging evidence suggests that the immunophenotype of cancer can be defined by components in the TIME, thereby influencing the prognosis of patients [8,10]. Myeloid-derived suppressor cells (MDSCs) in the TIME can improve invasion, angiogenesis, and metastasis formation, and suppress antitumor immunity [11]. In addition to immune cells, stromal cells can also modulate tumor immunophenotypes, like cancer-related fibroblasts, exerting a direct immunosuppressive mechanism of action [12]. As TIME plays a critical role in the tumorigenic process, the assessment of TIME status may be an effective method for predicting treatment benefits and patient prognosis.

Recent advances in genome sequencing and bioinformatics have provided useful tools for assessing TIME status based on gene expression data [13]. Based on massive genetic data from public databases (The Cancer Genome Atlas (TCGA), Immunology Database and Analysis Portal (ImmPort), Gene Expression Omnibus (GEO), and International Cancer Genome Consortium (ICGC)) and bioinformatics analysis methods, a comprehensive prognostic signature related to immune genes was constructed in this study, and the relationship between TIME and immunotherapy response with the riskscore model was explored. Additional immunohistochemistry experiments were used to validate the reliability of this immune-prognostic signature. In a nutshell, a risk score is the generation of an easily calculable number (score) that reflects the level of risk in the presence of certain risk factors. This prognostic signature is a risk score consisting of three genes (CD79a molecule (CD79A), Dickkopf WNT signaling pathway inhibitor 1 (DKK1), and vascular endothelial growth factor C (VEGFC)). Risk score $= \sum \beta i * Expi$, where βi is the coefficient of each gene and Expi is the normalized count of each hub gene. In addition, relevant algorithms and online analysis tools were applied to calculate immune, stromal, and estimated scores, to analyze the expression of immune checkpoint molecules, to map the landscape of tumor mutation burden, and to predict the response to immune checkpoint blockade (ICB) therapy and different medications in patients with different risk scores.

2. Materials and methods

2.1. Data sources and risk model analysis

The Genomic Data Commons Data Portal (https://portal.gdc.cancer.gov/projects/TCGA-LUAD, March 25, 2022) provides access to TCGA RNA-seq data, phenotype data, and survival data for LUAD patients [14]. Immune marker genes were collected from the ImmPort database [15] (https://www.immport.org/shared/genelists, February 28, 2022). Prognostic-related genes were studied and risk scores were calculated based on the TCGA dataset. GEO database (GSE68465) [16] (https://www.ncbi.nlm.nih.gov/geo/query/acc.cgi?acc=GSE68465, April 28, 2022) and ICGC LUAD database [17] (https://dcc.icgc.org/releases/current/Projects/LUAD-US, May 1, 2022) contain RNA-seq data and associated clinical information for externally independent validation datasets. The R package "DESeq2" [18] was adopted to identify differentially expressed genes (DEGs) using gene transcription profiles ($|\log2(\text{fold change})| > 1.2$, $P < 0.05$). DEGs and immune marker genes were intersected to obtain immune-related DEGs. The R package "cluster Profiler" [19] was used to determine the potential functions of these immune-related DEGs by Kyoto Encyclopedia of Genes and Genomes (KEGG) enrichment pathway analysis and Gene Ontology (GO) annotation [20,21].

2.2. Establishment and verification of a risk score model for prognosis

These overlapping immune-associated genes were applied to determine hub genes and build a risk score model for prognosis. The

immune genes associated with prognosis were screened using the univariate Cox proportional hazards regression. To avoid overfitting, all genes were analyzed by the "glmnet" [22] package for Lasso regression analysis. After the Lasso model filtering, these genes were analyzed using the multivariable Cox proportional hazards regression to develop this immune-related risk score model. Risk score = $\sum \beta_i$*Exp_i, where β_i is the coefficient of each gene and Exp_i is the normalized count of each hub gene [23]. Patients were categorized as low-risk or high-risk using the median risk score as the dividing line. Finally, the predictive power of this analytic model was assessed by the time-dependent receiver operating characteristic (ROC) curves and Kaplan-Meier (KM) survival curves. Then, the validation set (ICGC LUAD cohort and GSE68465 cohort) was used to verify the predictive ability and robustness of the risk model by KM survival curves and ROC curves.

2.3. The independent prognostic value of marker genes and their validation

With the help of univariate Cox, Lasso and multivariate Cox regression analysis, a risk score model was successfully established. The "pheatmap" [24] package was applied to create a heat map of the relationship between hub gene expression and the risk score model. An analysis of the relationship between survival time and the risk score model was performed using the "survminer" [25] package to generate a Kaplan-Meier diagram of these genes. The relationship between hub genes and risk scores was also examined, which was confirmed using a correlation scatter diagram.

2.4. The relationship between clinical factors and risk scores and gene set enrichment analysis of the risk model

First, the risk scores for clinical characteristics were compared in subgroups. Second, the impact of clinical factors on prognosis was evaluated using univariate and multivariate Cox regression to screen for significant clinical factors. The "rms" [26] package was used to create a nomogram according to therapy, stage, and risk score. Lastly, the prediction effects of the nomogram were verified based on the ROC curve and the calibration chart. On the basis of the GSEA software supplied by MsigDB, the gene set "c2. cp.kegg.v7.5. symbols.gmt" [27,28] (http://www.gsea-msigdb.org/gsea/msigdb/index.jsp, March 4, 2022) was selected as a reference gene set for determining the function of gene sets between low-risk and high-risk groups. FDR q-value <0.25 and NOM p-value <0.05 were considered as statistically significant.

2.5. Analysis of tumor immune signatures based on the risk model

The CIBERSORT algorithm [29] was used to analyze the proportion of immune cells in both low-risk and high-risk groups, and to investigate the expression levels of immune checkpoints in each group. ESTIMATE [30] is an algorithm that scores the proportion or abundance of immune, stromal, and tumor cells in the TIME given the transcriptional profile of tumor samples. In addition, a subgroup analysis of immune scores was conducted among LUAD patients with varying tumor stages, and how LUAD patients respond to immune checkpoint inhibitor therapy was predicted by using RNA-Seq data and the ImmuCellAI network analysis platform [31] (http://bioinfo.life.hust.edu.cn/ImmuCellAI#!/, May 25, 2022).

2.6. Analysis of tumor mutation status and key drug sensitivity

Information regarding somatic mutations was retrieved from the Genomic Data Commons Data Portal (https://portal.gdc.cancer.gov/projects/TCGA-LUAD, March 25, 2022). Using the "maftools" [32] package, the landscape of tumor mutation burden (TMB) and significantly mutated genes ($P < 0.05$) was analyzed in both low-risk and high-risk groups. The 50% maximal inhibiting concentration (IC50) values of eight common lung cancer drugs were calculated using the "pRRophetic" [33] package and compared by group ($P < 0.05$). In general, a greater IC50 value indicates a more sensitive response to drug treatment.

2.7. Clinical specimens and immunohistochemical staining analysis

We collected surgical specimens from 30 lung adenocarcinoma patients at our institution, made sections after paraffin fixation, sectioning, staining, incubation of antibodies, dehydration, and other steps, and then took photographs using a panoramic section scanner. Per section, the diagnosis was lung adenocarcinoma. Lung cancer tissues and adjacent normal tissues (<3 cm away from the tumor) were named as tumor group and adjacent normal group, respectively, and finally the proportion of positive cells in each picture was calculated by "" ImageJ "". (blue, negative; light yellow, weakly positive; brown yellow, moderately positive; dark brown, strongly positive; scale bar = 50 μm).

2.8. Statistical analysis

In Kaplan-Meier curve analysis, the log-rank test was used to compare statistical overall survival (OS) differences. The impact of single and multiple parameters on patient survival was evaluated by univariate and multivariate Cox regression analysis. If the two independent samples are paired samples, the Wilcoxon test can be chosen to compare the difference between the two datasets; otherwise, the Mann-Whitney test is utilized. The Kruskal-Wallis test was employed to assess the statistical difference in the distribution among three or more groups. The Spearman method was employed to compute the correlation coefficient and P value when investigating the correlation between the risk score and other factors. AUC values and nomogram scores were employed to evaluate the

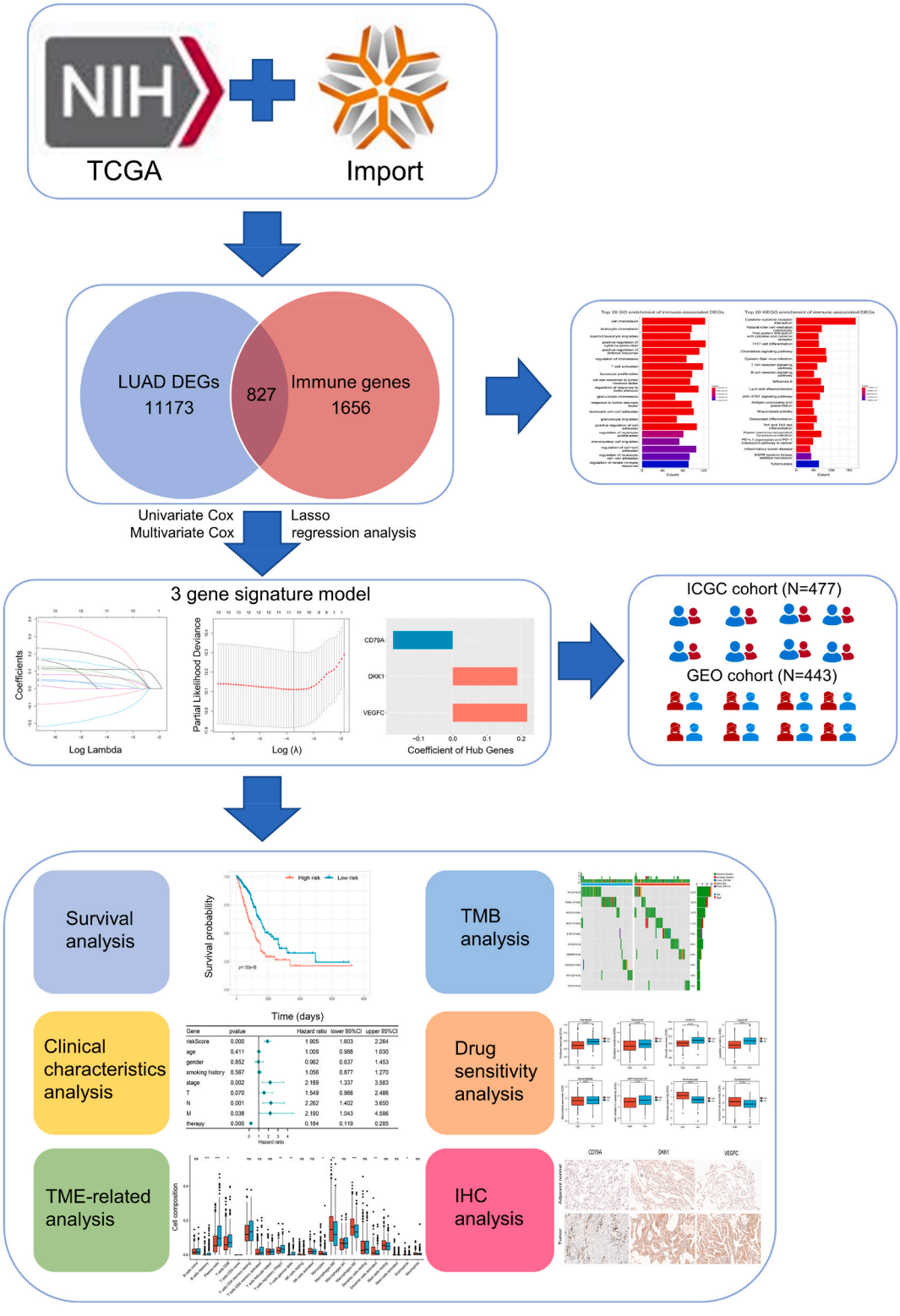

Fig. 1. Flowchart of the present study.

risk model's ability to predict overall survival incidence. The accuracy improves with increasing values of these two metrics. Only patients with complete relevant information were included in each of the aforementioned investigations. The R programming language (version 4.1.1) was used for data analysis and charting. Unless otherwise specified, *P*-value is two-sided, and $P < 0.05$ is statistically significant.

3. Results

3.1. Identification and annotation of immune-associated genes in LUAD patients

The implementation roadmap of this study is shown in Fig. 1, and the clinical characteristics of lung adenocarcinoma patients from different datasets with required survival and clinical information are shown in Table 1. The TCGA-LUAD project contained 58 normal and 510 tumor samples. Using the "DESeq2" package, a total of 12,000 differential genes were collected, of which 7397 differential genes were up-regulated and 4603 differential genes were down-regulated (Fig. 2A). The heat map depicts the profile differences between the normal and cancer groups (Fig. 2B). Two thousand, four hundred and eighty-three immune marker genes were obtained from the ImmPort database to identify immune-associated DEGs, and the intersection results revealed 827 immune-associated DEGs. The results of the KEGG and GO enrichment analyses of these selected immune DEGs were statistically significant ($P < 0.05$). Some of the most abundant enriched pathways or functional sets are closely related to immune regulation, such as "activation of B and T cells", "positive regulation of inflammatory factors", "natural killer cell-mediated cytotoxicity", and "PD-1 checkpoint pathway and PD-L1 expression in cancer", implying that the influence of different immune states on LUAD prognosis may be associated with immune pathway activation (Fig. 2C and D).

3.2. Development and validation of predictive signals based on immune-related genes

Based on immune-related DEGs, univariate Cox analysis identified thirteen genes that were highly related to overall survival (OS) in samples with survival information ($P < 0.001$) (Supplementary Fig. 1). Then, these genes were included in stepwise Lasso analysis, and multivariate cox regression analysis was performed to further narrow gene screening (Fig. 3A and B). According to multivariate

Table 1
Clinical characteristics of the LUAD patients used in this study.

Characteristic	Training dataset	Validation dataset	
	TCGA-LUAD	GSE68465-LUAD	ICGC-LUAD
Total	n = 497	n = 443	n = 477
Survival status			
Alive	317 (63.7%)	207 (46.7%)	359 (75.3%)
Dead	180 (36.3%)	236 (53.3%)	118 (24.7%)
Age			
≤ 65	236 (47.5%)	231 (52.1%)	215 (45.1%)
> 65	251 (50.5%)	212 (47.9%)	243 (50.9%)
Unknown	10 (2.0%)	0 (0.0%)	19 (4.0%)
Gender			
Male	228 (45.8%)	223 (50.3%)	220 (46.1%)
Female	269 (54.2%)	220 (49.7%)	257 (53.9%)
Stage			
I	267 (53.7%)	NA	NA
II	118 (23.7%)	NA	NA
III	80 (16.1%)	NA	NA
IV	25 (5.0%)	NA	NA
Unknown	7 (1.5%)	NA	NA
T stage			
T1	166 (33.4%)	150 (33.8%)	NA
T2	267 (53.7%)	251 (56.7%)	NA
T3	43 (8.7%)	28 (6.3%)	NA
T4	18 (3.6%)	12 (2.7%)	NA
Unknown	3 (0.6%)	2 (0.5%)	NA
N stage			
N0	321 (64.6%)	299 (67.5%)	NA
N1	94 (18.9%)	88 (19.8%)	NA
N2	69 (13.8%)	53 (12.0%)	NA
N3	2 (0.5%)	0 (0.0%)	NA
Unknown	11 (2.2%)	3 (0.7%)	NA
M stage			
M0	331 (66.6%)	NA	NA
M1	24 (4.8%)	NA	NA
Unknown	142 (28.6%)	NA	NA

Only patients with complete relevant information were included in each of the aforementioned investigations.

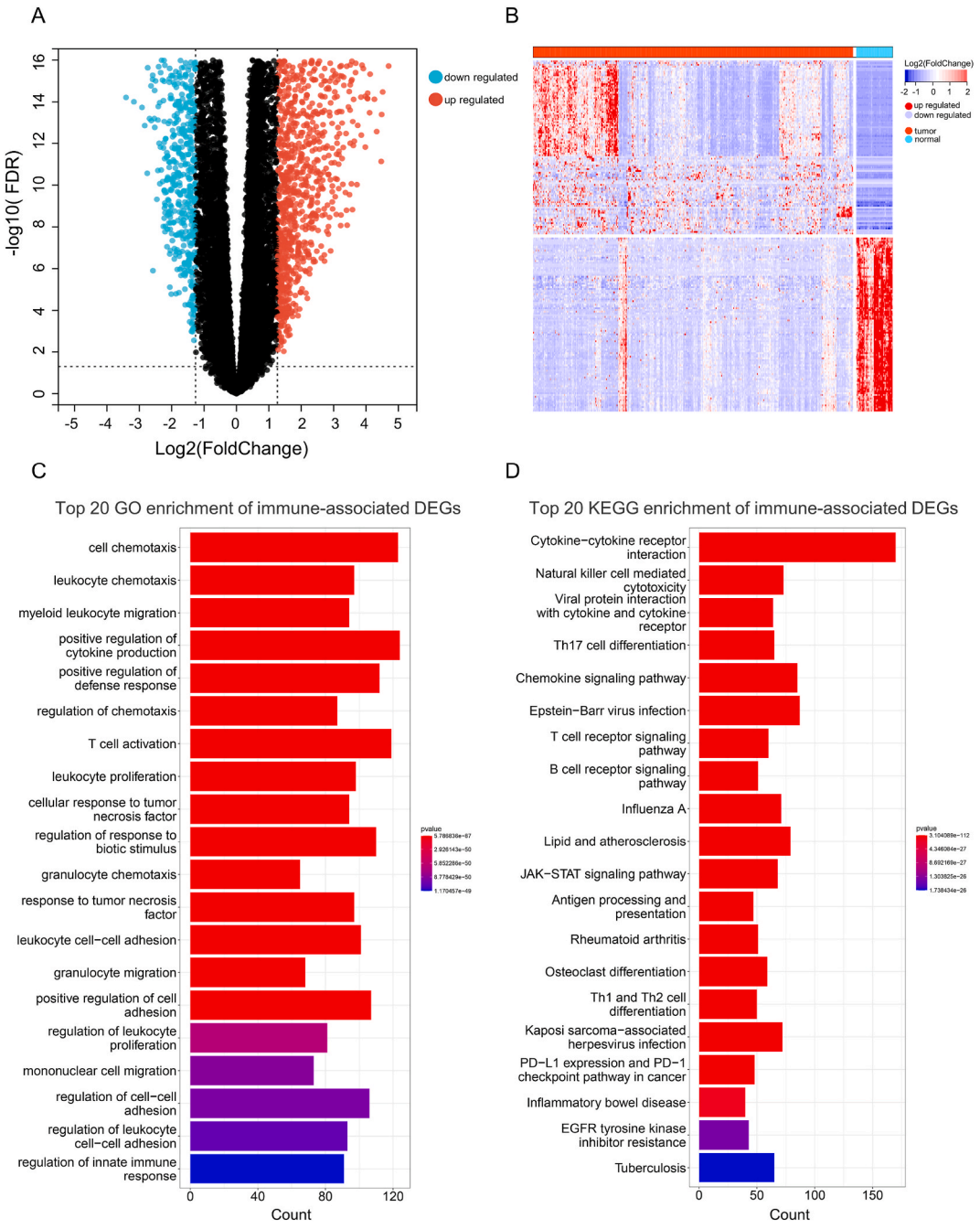

Fig. 2. Identification and annotation of immune-associated DEGs. (A) Volcano plot and (B) Heat map of DEGs based on TCGA-LUAD data. (C) Top 20 GO analyses of immune-related DEGs. (D) Top 20 most enriched KEGG pathways of immune-related DEGs.

Cox regression analysis, three immune-related DEGs were finally identified to develop the model ($P < 0.05$) (Figs. 3C and 4A). Then, CD79A, DKK1, and VEGFC were characterized for the construction of prognostic model as follows: Risk score = (−0.1743 * expression level of CD79A) + (0.1883 * expression level of DKK1) + (0.2175 * expression level of VEGFC) (Supplementary Table 1). Patients were categorized as low-risk or high-risk by taking the median risk score as the cut-off number. Based on the Kaplan-Meier analysis of TCGA, ICGC and GSE68465 groups, the survival of patients in the low-risk group was markedly higher than those in the high-risk group ($P < 0.05$) (Fig. 3D, E, G, H, J, K). The reliability of the risk model for 1-, 3-, and 5-year survival predictions in each group of patients was expressed as the area under the curve (AUC) (Fig. 3F, I, L). It is easy to understand that the average prediction efficiency of risk-score is almost always higher than 0.600 in all cases of the cohort indicating that the prediction results were more reliable.

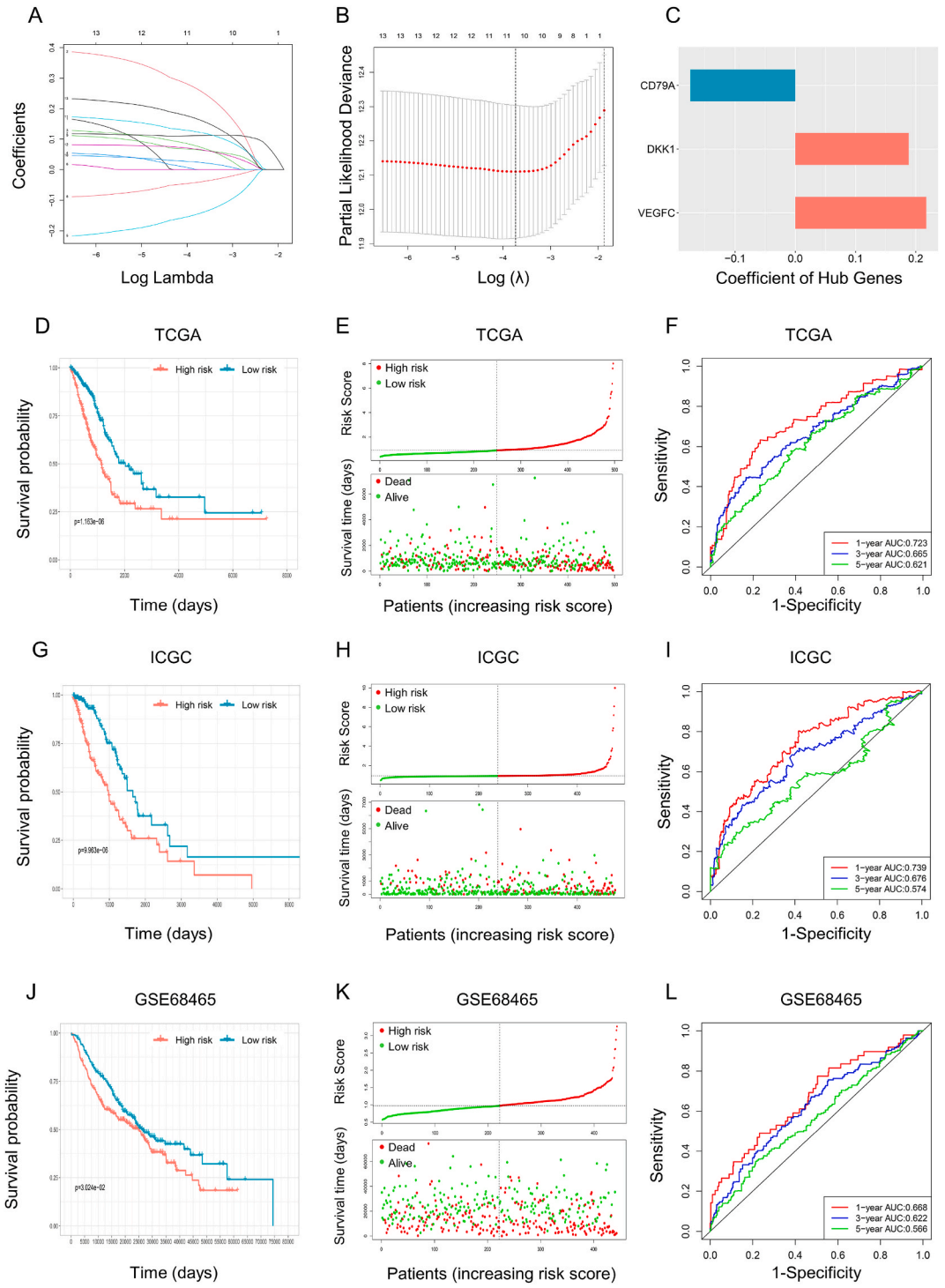

Fig. 3. The development and validation of a risk score model. (A) LASSO coefficient profile. (B) Selection of tuning parameters in the LASSO model using 10-fold cross-validation with minimal OS criterion. (C) Coefficients of the three chosen genes. (D) OS of the TCGA group. (E) Distribution of OS and risk score in TCGA. (F) Validation of survival-dependent ROC curves for prognostic indexes at 1, 3, and 5 years in TCGA. (G) OS of the ICGC group. (H) Distribution of OS and risk score in ICGC. (I) Validation of survival-dependent ROC curves for prognostic indexes at 1, 3, and 5 years in ICGC. (J) OS of the GSE68465 group. (K) Distribution of OS and risk score in GSE68465. (L) Validation of survival-dependent ROC curves for prognostic indexes at 1, 3, and 5 years in GSE68465.

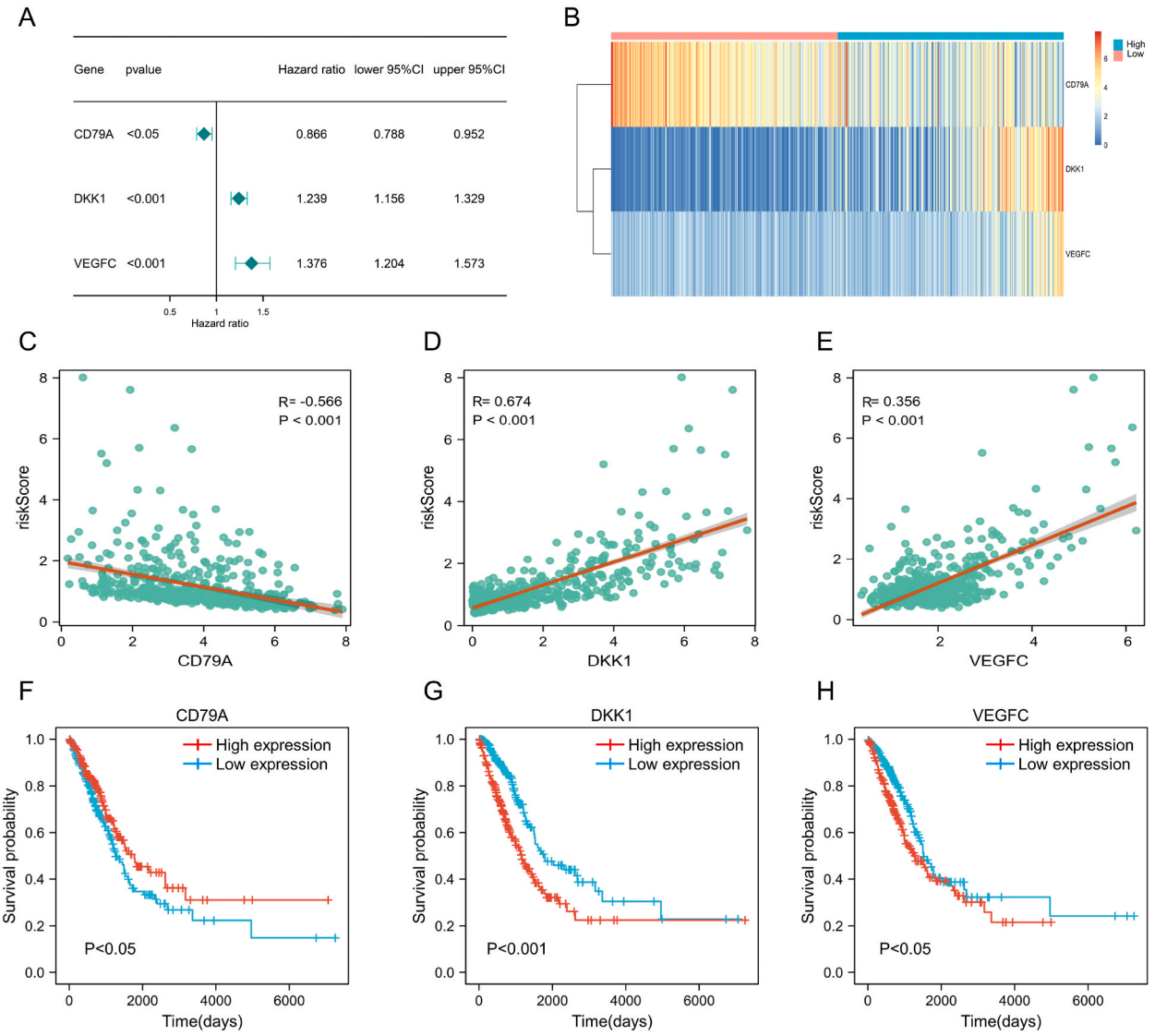

Fig. 4. Independent prognostic validation of the three signature genes. (A) Forest plot by multivariate Cox regression analysis of TCGA data. (B) Heatmap of the three signature genes based on the risk score. (*C*–E) Scatter plots of the correlation between risk score and three signature genes. (F–H) Kaplan-Meier survival curves of the three signature genes based on TCGA-LUAD data.

3.3. Independent prognostic validation of the three signature genes

The multivariate Cox regression analysis illustrated the role of independent prognostic value of these three signature genes (Fig. 4A). The cluster heatmap of the three genes showed higher expression of DKK1 and VEGFC in the high-risk group and higher expression of CD79A in the low-risk group (Fig. 4B). According to the correlation study of gene expression and risk score, the greater the expression of CD79A, the lower the risk score, and the higher the expression of DKK1 and VEGFC, the higher the risk score ($P < 0.001$) (Fig. 4C, D, E). The prognostic value of each signature gene was continually evaluated by building Kaplan-Meier survival curves. There were statistically significant differences in the distribution of survival time for CD79A, and the higher expression group had a better prognosis ($P < 0.05$) (Fig. 4F). The difference in the survival time distribution of DKK1 and VEGFC was statistically significant, although the higher expression group had worse prognosis ($P < 0.05$) (Fig. 4G and H), demonstrating that Kaplan-Meier survival outcomes agreed with the results of multivariate Cox regression analysis.

3.4. Correlation of clinical characteristics with the risk model

Clinical factors affecting prognosis in LUAD were assessed to validate the relationship with the risk model. In the Wilcoxon grade sum test, greater risk scores correspond to higher tumor grades and more advanced TNM stages, and patients with stable recovery have

a lower risk score than those with advanced cancer ($P < 0.05$) (Fig. 5A–H). The univariate and multivariate COX analysis was used to determine three independent prognostic markers (risk score, stage, and therapy) ($P < 0.05$), and then a nomogram model was developed to predict the survival of LUAD patients (Fig. 5I, J, K). The 1-, 3-, and 5-year AUC value for LUAD patients were 0.860, 0.721, and 0.706, respectively (Fig. 5L). The actual and expected survival rates of the calibration curve demonstrated that the prediction accuracy of this model was reliable (Fig. 5M, N, O).

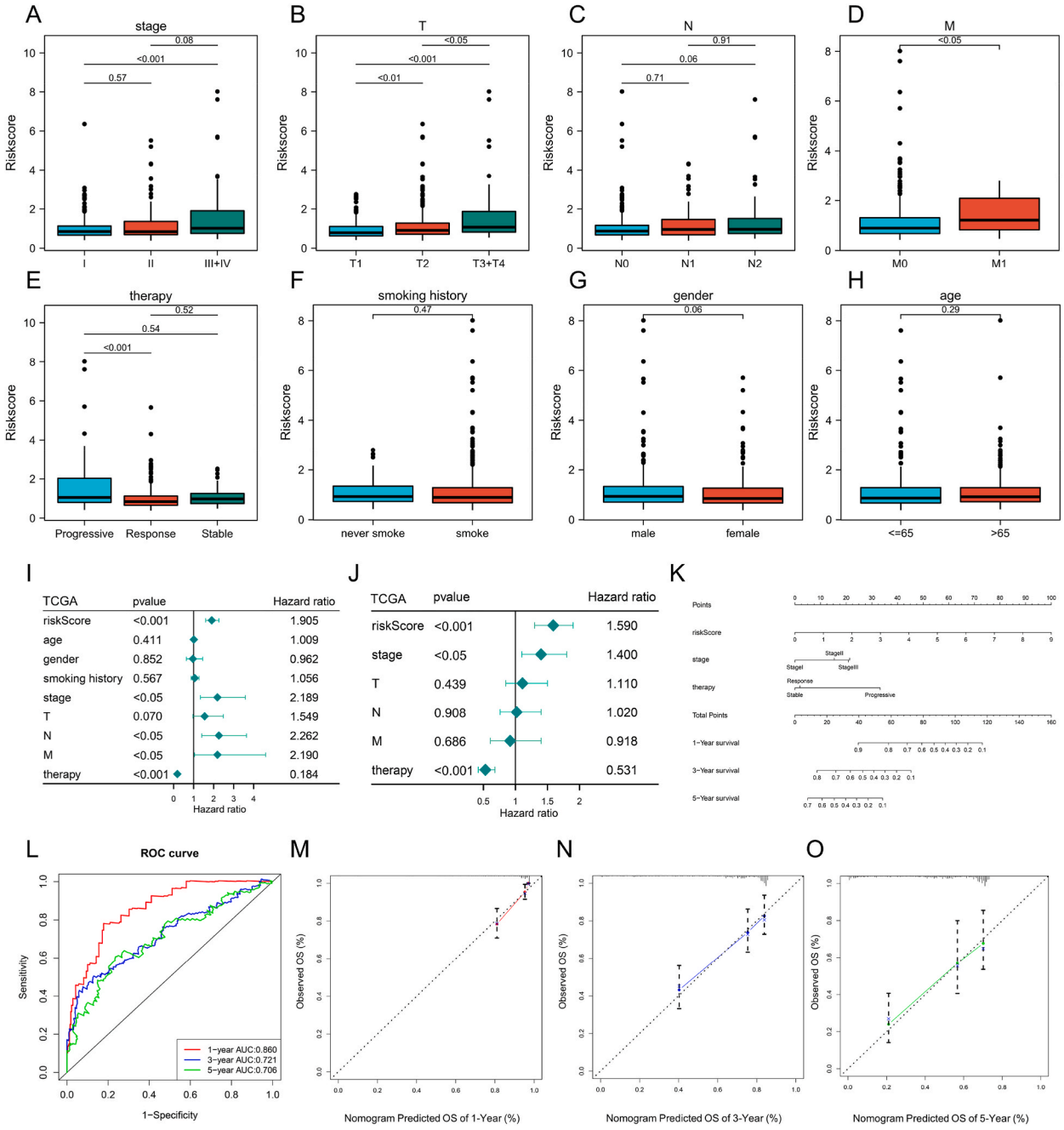

Fig. 5. Correlation between clinical characteristics and the risk model using the TCGA-LUAD group as the basis. Analysis of clinical factors and risk scores revealed that risk scores were significantly correlated with (A) stage, (B) T category, (D) metastasis, and (E) therapy outcome, but not with (C) lymph node invasion, (F) smoking history, (G) gender, or (H) age. (I) Univariate survival analysis of clinical characteristics. (J) Multivariate survival analysis of clinical characteristics. (K) Nomogram for predicting OS of LUAD patients. (L) Time-dependent ROC of the OS-based nomogram. (*M*–O) Calibration plots for internal validation of the nomogram.

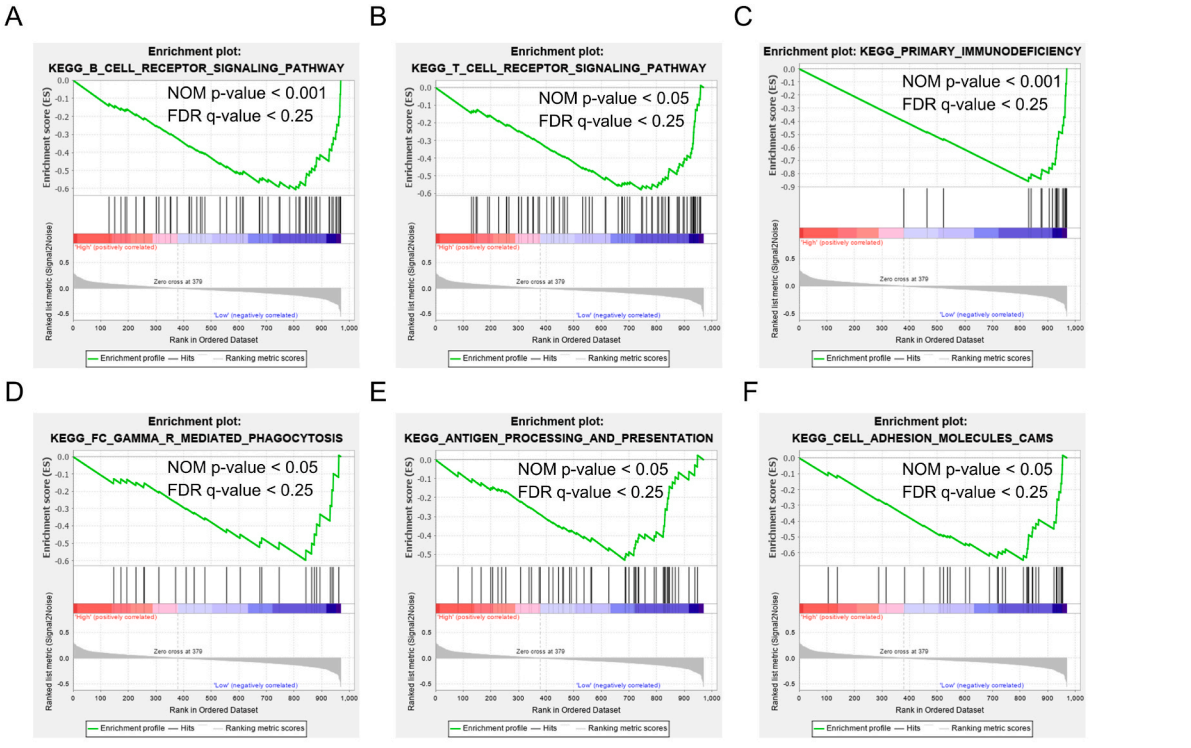

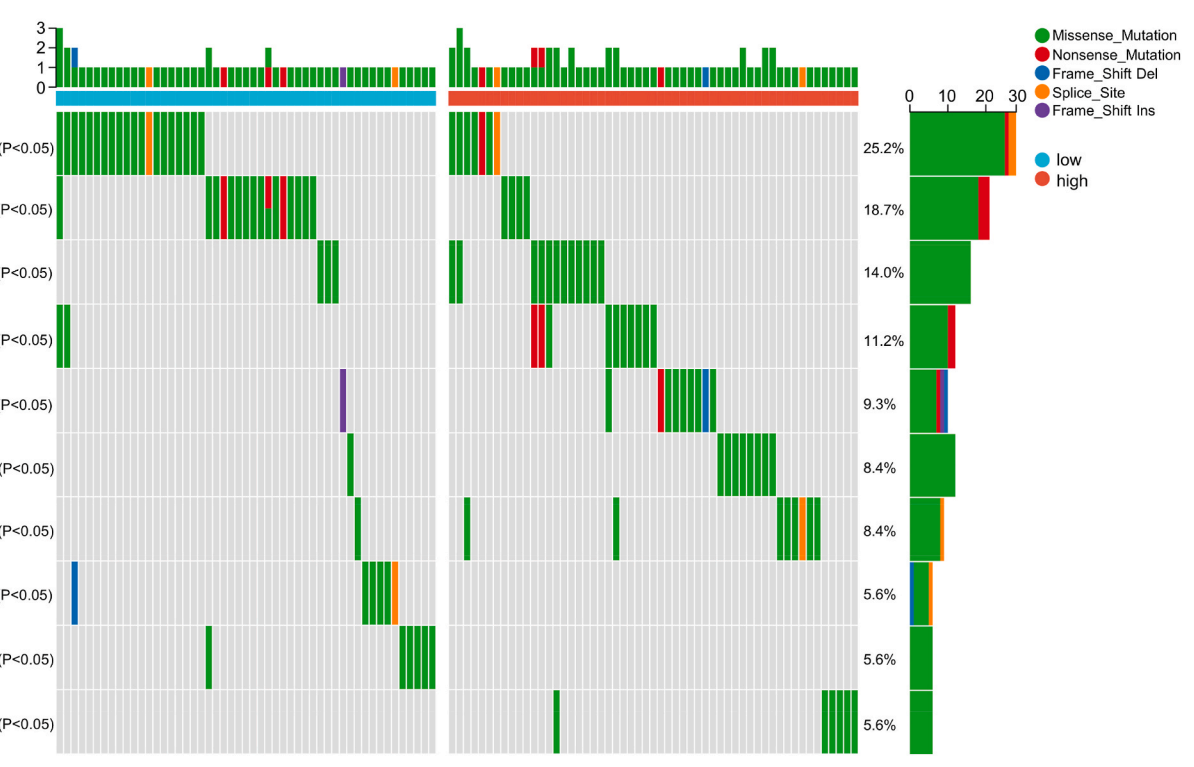

(caption on next page)

Fig. 6. Plots of immune-related gene sets based on GSEA and the landscape of mutant genes from patients with LUAD in low-risk and high-risk groups. The images show gene sets in (A) B cell receptor signaling pathway, (B) T cell receptor signaling pathway, (C) Primary immunodeficiency, (D) Fc gamma R-mediated phagocytosis, (E) Antigen processing and presentation, and (F) Cell adhesion molecules (CAMs). (G) Waterfall plot depicts the mutation difference of mutant genes in each group. The color blue indicates LUAD patients at low risk, whereas the color red represents LUAD patients at high risk. The upper bar plot represents the tumor mutation burden (TMB). The left p value shows the statistical difference between the two groups. The right number represents the frequency of mutation in each gene. The proportion of each variation type is indicated by the color of the bar graph on the right.

3.5. Immune-associated gene enrichment analysis in the risk model

A GSEA enrichment analysis was conducted on the immune-associated gene to further examine the molecular function of this polygenic prognostic signature model in the immune system. The identification results showed that only a few immune-related gene sets were enriched in the high-risk group, whereas the majority were enriched in the low-risk group (FDR q-value <0.25 and NOM p-value <0.05). Furthermore, the significant KEGG pathway-enriched gene sets all belonged to the low-risk category. The KEGG gene set enriched in the low-risk group was shown to participate in various immunological activities, such as B cells, T cells, antigen delivery, phagocytosis, cell adhesion molecules, and primary immunodeficiency (Fig. 6A–F). These results illustrated that the low-risk group in this risk model participated in more enriched immune processes than the high-risk group.

3.6. Relationship between the risk score model and TIME

To further investigate the immune microenvironment of LUAD, consistent results were obtained by examining the composition of immune cells and the expression of immune checkpoints in different risk groups. Activated DCs, M2 macrophages, M0 macrophages, monocytes and eosinophils had a higher degree of cell infiltration in high-risk patients ($P < 0.05$), while CD8 T cells, plasma cells, memory B cells, regulatory T cells and γδT cells had a higher degree of cell infiltration in low-risk patients ($P < 0.05$) (Fig. 7A). The immune checkpoints programmed cell death 1 receptor (PD1), cytotoxic T-lymphocyte associated protein 4 (CTLA4), lymphocyte activating 3 (LAG3), and indoleamine 2,3-dioxygenase (IDO) had a higher level of expression in low-risk patients ($P < 0.01$), while lemur tyrosine kinase 3 (LMTK3) and T cell immunoreceptor with Ig And ITIM domains protein (TIGHT) had a higher level of expression in high-risk patients ($P < 0.05$) (Fig. 7B). Immune infiltration and ICB treatment response scores were higher in the low-risk group ($P < 0.001$) (Fig. 7C, G). The ESTIMATE results showed that the high-risk group had a significantly lower immune score than the low-risk group ($P < 0.001$) (Fig. 7D, E, F). The lower the risk score, the higher the immune score ($P < 0.001$) (Fig. 7H, I, J). In the combined tumor staging analysis, the high-risk group had a significantly lower stromal score, immune score, and estimate score than the low-risk group in both stage and TNM staging subgroup analyses ($P < 0.05$) (Fig. 7K–V). Taking these data together, LUAD patients in the low-risk group had a higher level of immune response than those in the high-risk group.

3.7. Identification of tumor mutation burden in different risk groups

Key genes that were highly ranked by mutation frequency in tumor samples were filtered to make a compact gene mutation spectrum. The high-risk group had significantly lower mutation frequencies of neuregulin 3 (NRG3), trichohyalin like 1 (TCHHL1), CD40 ligand (CD40LG), and transcription factor 7 like 2 (TCF7L2) than the low-risk group ($P < 0.05$), while the low-risk group had significantly lower mutation frequencies of NEDD4 E3 ubiquitin protein ligase (NEDD4), MBL associated serine protease 1 (MASP1), sphingosine-1-phosphate receptor 1 (S1PR1), CD1c molecule (CD1C), colony stimulating factor 3 receptor (CSF3R), and nucleotide binding oligomerization domain containing 1 (NOD1) than the high-risk group ($P < 0.05$). Overall, the low-risk group had a significantly lower tumor mutation burden than the high-risk group (Fig. 6G).

3.8. Sensitivity of different drug treatments in the risk model

The risk model was used as a marker to observe the treatment response of LUAD patients to different drugs. IC50 is a quantitative index to evaluate the sensitivity of drug treatment. The pRRophetic algorithm was used to screen IC50 of eight commonly used LUAD drugs. Low-risk patients were found to be more sensitive to paclitaxel, docetaxel, erlotinib, lapatinib, gemcitabine, and AKT inhibitor VIII ($P < 0.001$) (Fig. 8A–F), while high-risk patients were more sensitive to methotrexate and camptothecin ($P < 0.001$) (Fig. 8G and H). Combined with the previous analysis of immune infiltration in LUAD patients, low-risk patients had higher immune infiltration scores and higher drug sensitivity, suggesting that low-risk and hyper-immune patients have a better response to medical therapy.

3.9. Immunohistochemical analysis of CD79A, DKK1, and VEGFC

CD79A, DKK1, and VEGFC are important differential genes associated with the tumor immune microenvironment. To further confirm these results, we performed IHC analysis on pathological samples from LUAD volunteers. Representative images of CD79A, DKK1, and VEGFC immunostaining in cancer tissues and paracancerous tissues are shown in Fig. 8I, J, K. In Fig. 8I, those negatively labeled in light blue are tumor cells, and those positively labeled in brown by CD79A are B lymphocytes, located in interstitial sites. This result illustrated that the proportion of CD79A labeled B lymphocytes was significantly higher than that of adjacent normal groups, and CD79A was related to the infiltration of B cells in the tumor microenvironment ($P < 0.01$) (Fig. 8L). CD19, as another

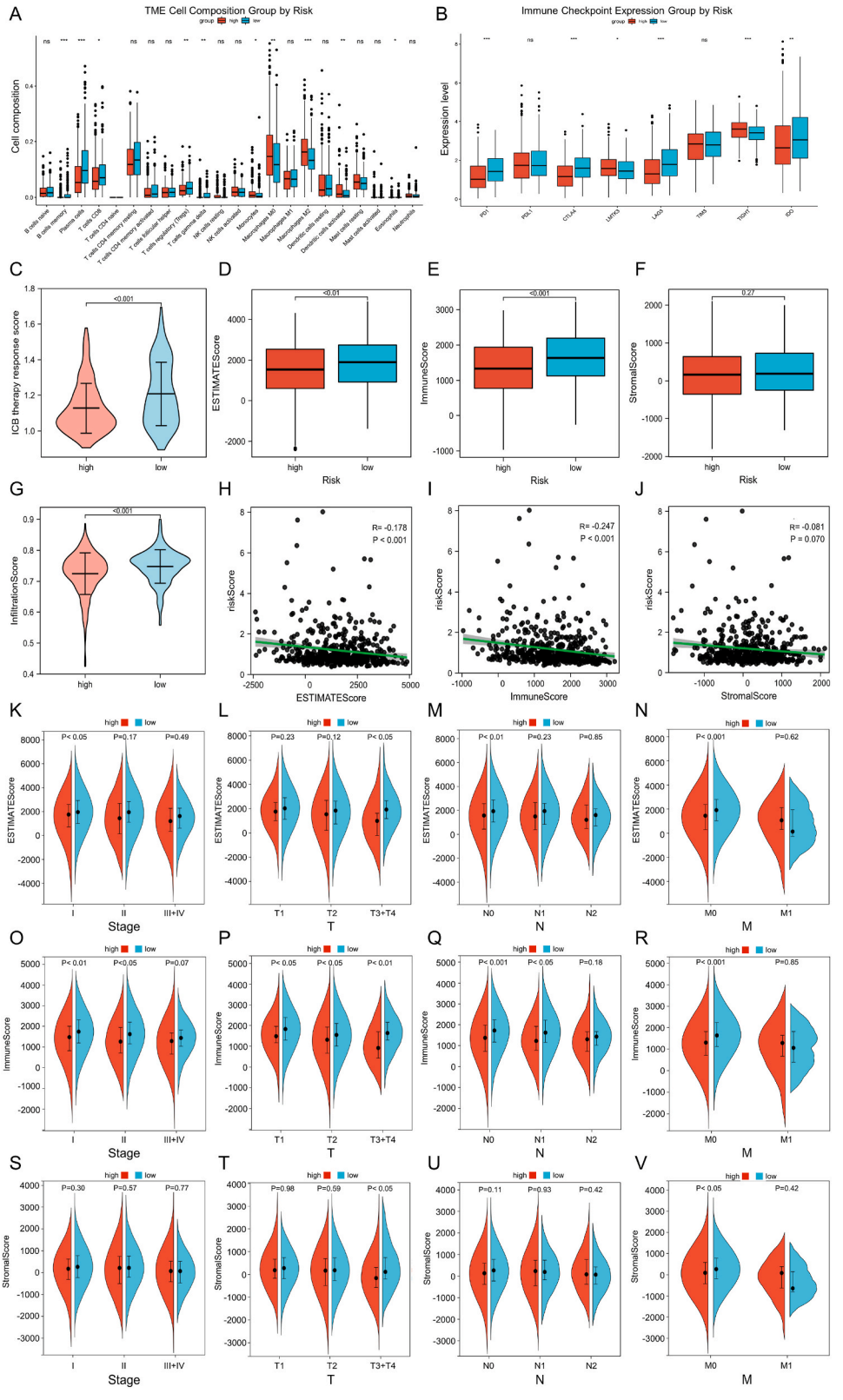

(caption on next page)

Fig. 7. Relationship between immune status and risk model. (A) Comparative analysis of the infiltration degree of 22 immune cells in low-risk and high-risk groups. (B) Analysis of the differential expression of 8 immune checkpoints in low-risk and high-risk groups. (C) Comparison of ICB therapy response score in low-risk and high-risk groups. (D–F) Differences in the expression of the stromal score, immune score, and ESTIMATE score in low-risk and high-risk groups. (G) Comparison of immune infiltration score in low-risk and high-risk groups. (H–J) Relationship between risk score and stromal score, immune score, and ESTIMATE score. (K–N) Comparison of ESTIMATE score across TNM stages and stage subgroups. (*O*–R) Comparison of immune score across TNM stages and stage subgroups. (*S*–V) Comparison of stromal score across TNM stages and stage subgroups. *P < 0.05, **P < 0.01, ***P < 0.001 compared between the groups.

different B cell marker, also showed that the proportion of B lymphocytes was significantly higher than that in the adjacent normal group (P < 0.01) (Supplementary Figs. 2 and 3). The results of CD3-labeled T-lymphocytes showed that T-lymphocyte infiltration in the tumor group was significantly higher than that in the adjacent normal group (P < 0.01) (Supplementary Figs. 4 and 5). In Fig. 8 J, K tumor cells proliferated primarily along the alveolar wall and were labeled brown yellow by DKK1 and VEGFC. The proportion of positive cancer cells labeled by DKK1 and VEGFC is significantly higher than that in the adjacent normal group (P < 0.001, P < 0.01) (Fig. 8M and N). The results demonstrated that DKK1 and VEGFC were tumor-specific and highly expressed in LUAD.

4. Discussion

In this work, a new risk score model was established and validated based on immune-associated genes. Our data indicate that the risk score is an independent predictor with a significant influence on the survival prediction of LUAD patients. Compared with high-risk patients, low-risk patients exhibited a lower tumor mutation burden, a higher immune score in both total and pathological staging subgroups, a greater response to targeted drugs and immune checkpoint blockade (ICB) therapy, and a longer survival rate. In addition, the majority of immunological checkpoints with immunotherapeutic potential were enriched in the lowest risk group. Given the distribution of ICB response scores and immune cells in low-risk and high-risk groups, the risk score may serve as a possible biomarker for predicting immunotherapy response and prognosis.

The application of the ESTIMATE algorithm to the computation of tumor gene expression profiles offers a quantitative way for evaluating the immunological state of tumor tissue [34]. There is a difference in the predictive value of high immune cell infiltration in various cancer types. Multiple researchers have categorized tumors as “hot” or “cool” by assessing the expression of tumor-infiltrating immune cells across 32 malignancies [35]. For “hot” tumors with very strong immune cell infiltration, high immune cell infiltration always has an association with a better prognosis [36], indicating that boosting immune cell infiltration as a treatment for malignancies may have beneficial consequences. In contrast, “cool” tumors with little or no immune cell infiltration often have an association with a poor prognosis, indicating that transforming “cool” tumors into “hot” tumors may sensitize patients to immunotherapy. In this study, low-risk patients had a higher immunological score and a better prognosis than high-risk patients. In light of this, it can be predicted that the treatment results may be improved if the degree of immune cell infiltration is increased in high-risk patients.

Tumor-infiltrating immune cells (TIICs) play a crucial role in both tumor growth and therapeutic response [37]. The composition of TIICs reflects anticancer immune response mechanisms and aids in the identification of novel prognostic characteristics. As a reliable indicator of patient prognosis, T cell infiltration has been utilized in treating a variety of malignancies [38]. Studies have revealed the favorable effect of T cells on tumor development [39], and mismanagement of T cells may result in immune evasion [40]. In the present investigation, high infiltration of CD8 T cells, regulatory T cells, and T cells was associated with a better prognosis, suggesting the therapeutic benefits of activating these cells in the TIME. B cells are essential immune system components that regulate the response of T cells by secreting cytokines and providing antigens [41]. High levels of memory B lymphocytes and plasma cells indicated a better prognosis in the current investigation. Several studies have found that MDSCs, such as macrophages, DCs, neutrophils, and eosinophils, are important contributors to immunosuppression in the TIME [42]. In this study, higher levels of monocytes, macrophages, activated dendritic cells, and eosinophils were detected in the high-risk group, which may be associated with the poor prognosis of high-risk patients.

The immune system is responsible for detecting and eliminating tumor cells. To avoid the immune attack, tumor cells frequently up-regulate the expression of immunosuppressive proteins, especially programmed death molecule 1 (PD1) and its ligand (PD-L1). These molecules inhibit the activation of immune cells and weaken the immune response [43]. Immune checkpoint inhibitor therapy involves the activation of immune effector cells, particularly B and T lymphocytes in the TIME, to kill tumor cells by inhibiting immunosuppressive proteins [44]. As treatment options for lung cancer, PD-L1 inhibitors (atezolizumab) and PD-1 inhibitors (pembrolizumab and nivolumab) have been listed successively as first-line or second-line drugs. Important clinical data revealed that atezolizumab, pembrolizumab, and nivolumab in advanced non-small cell lung cancer (NSCLC) exhibited significantly longer survival and manageable safety [45]. According to the results of an additional significant clinical trial, the median overall survival phase of nivolumab-treated stage III b/IV NSCLC patients treated with platinum-containing dual-drug chemotherapy was markedly longer than that of docetaxel-treated patients [46]. Iplimumab, a CTLA-4 inhibitor, is one of the first immunotherapeutic drugs for cancer in clinical trials. In lung cancer, ipilimumab monotherapy has not demonstrated significant efficacy, and a growing number of clinical trials are being conducted to evaluate its efficacy when combined with chemotherapy or other immunotherapies [47]. Compared to chemotherapy, the combination of nivolumab and iplimumab was found to increase the overall survival of patients with NSCLC [48]. Also, expression of PD1, CTLA4, and LAG3 was lower in high-risk patients, and ImmuCellAI calculations showed that high-risk patients had a poor response to ICB therapy. Therefore, it can be hypothesized that this may be related to the inability of some LUAD patients to achieve the anticipated efficacy after ICB treatment.

Tumor mutation burden (TMB) is the number of gene mutations present within the tumor. In general, the higher the TMB, the

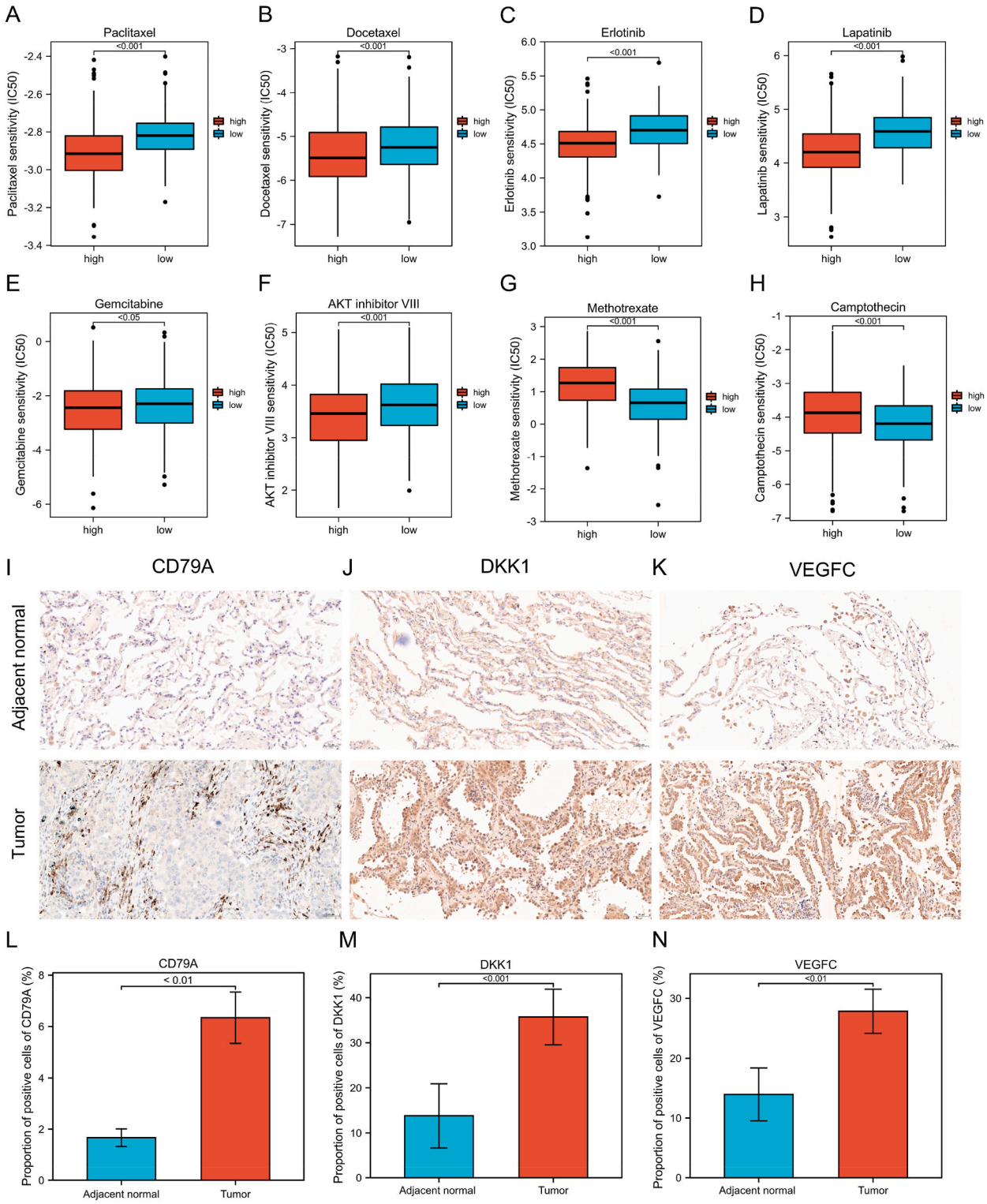

Fig. 8. Efficacy prediction of some important lung cancer drugs and expression of CD79A, DKK1, and VEGFC in tumor and adjacent normal tissues in LUAD patients from hospital samples. Boxplots of the comparison of IC50 values of (A) paclitaxel, (B) docetaxel, (C) erlotinib, (D) lapatinib, (E) gemcitabine, (F) AKT inhibitor VIII, (G) methotrexate, and (H) camptothecin in high-risk and low-risk groups. (I, L) IHC staining representation and proportion of CD79A in tumor and adjacent normal tissues (Scale bar = 50 μm). (J, M) IHC staining representation and proportion of DKK1 in tumor and adjacent normal tissues (Scale bar = 50 μm). (K, N) IHC staining representation and proportion of VEGFC in tumor and adjacent normal tissues (Scale bar = 50 μm).

greater the variety and number of neoantigens produced by tumor cells, the higher the probability of being recognized by the immune system, and the greater the probability of killing these tumor cells after immune checkpoint inhibitors activate the body's own antitumor immune response [49,50]. In the high-risk group, the higher incidence of mutations in NEDD4, MASP1, S1PR1, CD1C, CSF3R, and NOD1 is the primary cause of the elevated TMB. Whether unknown changes caused by the common mutations of these genes will affect the efficacy of tumor immunotherapy requires further research.

The predictive signature model includes CD79A, DKK1, and VEGFC. These genes serve as positive or negative prognosticators. CD79A encodes the Ig-alpha protein in the antigenic portion of B cells. Ig-alpha initiates a signal transduction cascade in the immune system by combining with Ig-beta, surface immunoglobulin (Ig), and B-cell antigen receptor (BCR). According to Zou Z, CD79A is positively correlated with the number of B lymphocytes in the TIME [51]. In a mouse model, Julamanee J discovered that the CD79 A/CD40 co-stimulatory domain can increase the proliferative capacity of CAR-T cells and enhance their antitumor effectiveness [52]. In this study, CD79A is an indicator of a favorable prognosis. With the increase of CD79A expression, the risk score decreases, the B lymphocyte infiltration increases, and the prognosis improves. As the Dickkopf WNT signaling pathway inhibitor 1, DKK1 has been reported to be elevated in numerous human cancers, making it an important research and treatment target for numerous tumor types [53]. Previous studies have demonstrated that DKK1 is a potent biomarker for multiple myeloma [54]. Lower expression of DKK1 is related to poor prognosis in KIRC and ESCA, whereas higher expression of DKK1 is related to poor prognosis in stomach adenocarcinoma (STAD), pancreatic adenocarcinoma (PAAD), mesothelioma (MESO), lung adenocarcinoma (LUAD), acute myeloid leukemia (LAML), head and neck squamous cell carcinoma (HNSC), and adrenocortical carcinoma (ACC) [55]. Some research suggests that DKK1 can promote the invasion and migration of NSCLC cells [56], while other research indicates that DKK1 can suppress the invasion and migration of breast cancer cells [57]. Identifying the two-sided action of DKK1 has the potential to serve as a prognostic marker for a variety of cancers. The VEGFC gene-encoding protein is a member of the vascular endothelial growth factor/platelet-derived growth factor (VEGF/PDGF) family, promoting endothelial cell growth, angiogenesis, and vascular permeability. This gene has been reported to stimulate tumor proliferation and migration and to influence tumor vascular permeability [58]. In addition, VEGFC has been considered to be an immunomodulator that modifies the immune system, thereby making it easier for tumor cells to evade immune surveillance [59]. Patients with moderate to high VEGFC expression have a lower survival rate of NSCLC [60]. In this study, DKK1 and VEGFC are both highly expressed in tumor tissue and are thought to be poor prognostic indicators. The risk score is positively correlated with DKK1 and VEGFC. The lower the survival rate of patients with LUAD, the more DKK1 and VEGFC are expressed.

This research had certain limitations. First, the data utilized for analysis at that time were only downloaded from public databases, and the sample size and completeness of patient information were limited by the time the database was updated. Second, immune infiltration scores and immune cell proportions in the tumor microenvironment are the product of complex algorithmic calculations; hence, their prediction of the immunotherapy response is indirect. Third, multiple mechanisms influence the occurrence and progression of lung adenocarcinoma, and while we collected 30 cancer human tissue samples for immunohistochemistry assay to validate this study, the molecular mechanisms of these genes with lung adenocarcinoma require additional functional experiments to be elucidated. In the future, an increase in the number of well-designed, multicenter, integrated clinical bioinformatics research projects will allow for a more complete confirmation of our findings.

5. Conclusion

In conclusion, this is the first study to develop a prognostic prediction model for LUAD patients based on CD79A, DKK1, and VEGFC. Functionally, the risk score was associated with TIME, overall survival, and medication treatment in LUAD patients. The excellent performance of this risk model indicates its robust and extensive application potential.

Ethical statement

This study was done in compliance with the Helsinki Declaration and was authorized by the ethics committee of Zhejiang Hospital under ethical review number 2022(89 K)-X1. All patients provided informed consent.

Author contribution statement

Qilong Zhang: Conceived and designed the experiments; Performed the experiments; Analyzed and interpreted the data; Wrote the paper.

Mingyuan Zhao; Shuangyan Lin: Performed the experiments; Contributed reagents, materials, analysis tools or data; Wrote the paper.

Qi Han; He Ye: Performed the experiments.

Fang Peng: Contributed reagents, materials, analysis tools or data.

Li: Contributed reagents, materials, analysis tools or data; Wrote the paper.

Funding statement

This work was supported by the Natural Science Foundation of Zhejiang Province (LQ15H310003) and the key disciplines of Zhejiang Hospital (Z210071).

Data availability statement

Data will be made available on request.

Declaration of competing interest

The authors declare that they have no known competing financial interests or personal relationships that could have appeared to influence the work reported in this paper.

Appendix A. Supplementary data

Supplementary data to this article can be found online at https://doi.org/10.1016/j.heliyon.2023.e18503.

References

[1] B.C. Bade, C.S. Dela Cruz, Lung cancer 2020: epidemiology, etiology, and prevention, Clin. Chest Med. 41 (1) (2020) 1–24, https://doi.org/10.1016/j.ccm.2019.10.001.
[2] F. Nasim, B.F. Sabath, G.A. Eapen, Lung cancer, Med. Clin. 103 (3) (2019) 463–473, https://doi.org/10.1016/j.mcna.2018.12.006.
[3] A.L. Oliver, Lung cancer: epidemiology and screening, Surg. Clin. 102 (3) (2022) 335–344, https://doi.org/10.1016/j.suc.2021.12.001.
[4] D.S. Ettinger, et al., Non–small cell lung cancer, version 3.2022, NCCN clinical practice guidelines in oncology, J. Natl. Compr. Cancer Netw. 20 (5) (2022) 497–530, https://doi.org/10.6004/jnccn.2022.0025.
[5] T. Li, et al., Genotyping and genomic profiling of non-small-cell lung cancer: implications for current and future therapies, J. Clin. Oncol. 31 (8) (2013) 1039–1049, https://doi.org/10.1200/jco.2012.45.3753.
[6] Z. Wang, et al., Identifying M1-like macrophage related genes for prognosis prediction in lung adenocarcinoma based on a gene co-expression network, Heliyon 9 (1) (2023), e12798, https://doi.org/10.1016/j.heliyon.2023.e12798.
[7] D. Chen, et al., Metabolic regulatory crosstalk between tumor microenvironment and tumor-associated macrophages, Theranostics 11 (3) (2021) 1016–1030, https://doi.org/10.7150/thno.51777.
[8] D.C. Hinshaw, L.A. Shevde, The tumor microenvironment innately modulates cancer progression, Cancer Res. 79 (18) (2019) 4557–4566, https://doi.org/10.1158/0008-5472.can-18-3962.
[9] Y. Xiao, D. Yu, Tumor microenvironment as a therapeutic target in cancer, Pharmacol. Ther. 221 (2021), 107753, https://doi.org/10.1016/j.pharmthera.2020.107753.
[10] H. Choi, K.J. Na, Integrative analysis of imaging and transcriptomic data of the immune landscape associated with tumor metabolism in lung adenocarcinoma: clinical and prognostic implications, Theranostics 8 (7) (2018) 1956–1965, https://doi.org/10.7150/thno.23767.
[11] P. De Cicco, G. Ercolano, A. Ianaro, The new era of cancer immunotherapy: targeting myeloid-derived suppressor cells to overcome immune evasion, Front. Immunol. 11 (2020) 1680, https://doi.org/10.3389/fimmu.2020.01680.
[12] Z. Liao, et al., Cancer-associated fibroblasts in tumor microenvironment – accomplices in tumor malignancy, Cell. Immunol. 343 (2019), 103729, https://doi.org/10.1016/j.cellimm.2017.12.003.
[13] J. Zou, E. Wang, Cancer biomarker discovery for precision medicine: new progress, Curr. Med. Chem. 26 (42) (2019) 7655–7671, https://doi.org/10.2174/0929867325666180718164712.
[14] R.L. Grossman, et al., Toward a shared vision for cancer genomic data, N. Engl. J. Med. 375 (12) (2016) 1109–1112, https://doi.org/10.1056/NEJMp1607591.
[15] S. Bhattacharya, et al., ImmPort, toward repurposing of open access immunological assay data for translational and clinical research, Sci. Data 5 (1) (2018), 180015, https://doi.org/10.1038/sdata.2018.15.
[16] T. Barrett, et al., NCBI GEO: archive for functional genomics data sets–update, Nucleic Acids Res. 41 (2013) D991–D995, https://doi.org/10.1093/nar/gks1193 (Database issue).
[17] J. Zhang, et al., The international cancer genome Consortium data portal, Nat. Biotechnol. 37 (4) (2019) 367–369, https://doi.org/10.1038/s41587-019-0055-9.
[18] M.I. Love, W. Huber, S. Anders, Moderated estimation of fold change and dispersion for RNA-seq data with DESeq2, Genome Biol. 15 (12) (2014) 550, https://doi.org/10.1186/s13059-014-0550-8.
[19] G. Yu, et al., clusterProfiler: an R package for comparing biological themes among gene clusters, OMICS 16 (5) (2012) 284–287, https://doi.org/10.1089/omi.2011.0118.
[20] M. Kanehisa, et al., KEGG for taxonomy-based analysis of pathways and genomes, Nucleic Acids Res. 51 (D1) (2023) D587–D592, https://doi.org/10.1093/nar/gkac963.
[21] C. The Gene Ontology, The Gene Ontology resource: enriching a GOld mine, Nucleic Acids Res. 49 (D1) (2021) D325–D334, https://doi.org/10.1093/nar/gkaa1113.
[22] J.H. Friedman, T. Hastie, R. Tibshirani, Regularization paths for generalized linear models via coordinate descent, J. Stat. Software 33 (1) (2010) 1–22, https://doi.org/10.18637/jss.v033.i01.
[23] J. Wu, et al., A risk model developed based on tumor microenvironment predicts overall survival and associates with tumor immunity of patients with lung adenocarcinoma, Oncogene 40 (26) (2021) 4413–4424, https://doi.org/10.1038/s41388-021-01853-y.
[24] R. Kolde, Pheatmap: Pretty Heatmaps, 2019.
[25] A. Kassambara, M. Kosinski, P. Biecek, Survminer: Drawing Survival Curves Using, ggplot2, 2021.
[26] Jr, F.E.H., Rms: Regression Modeling Strategies, 2022.
[27] A. Subramanian, et al., Gene set enrichment analysis: a knowledge-based approach for interpreting genome-wide expression profiles, Proc. Natl. Acad. Sci. USA 102 (43) (2005) 15545–15550, https://doi.org/10.1073/pnas.0506580102.
[28] V.K. Mootha, et al., PGC-1α-responsive genes involved in oxidative phosphorylation are coordinately downregulated in human diabetes, Nat. Genet. 34 (3) (2003) 267–273, https://doi.org/10.1038/ng1180.
[29] A.M. Newman, et al., Robust enumeration of cell subsets from tissue expression profiles, Nat. Methods 12 (5) (2015) 453–457, https://doi.org/10.1038/nmeth.3337.
[30] K. Yoshihara, et al., Inferring tumour purity and stromal and immune cell admixture from expression data, Nat. Commun. 4 (1) (2013) 2612, https://doi.org/10.1038/ncomms3612.
[31] Y.-R. Miao, et al., ImmuCellAI: a unique method for comprehensive T-cell subsets abundance prediction and its application in cancer immunotherapy, Adv. Sci. 7 (7) (2020), 1902880, https://doi.org/10.1002/advs.201902880.

[32] A. Mayakonda, et al., Maftools: efficient and comprehensive analysis of somatic variants in cancer, Genome Res. 28 (2018), https://doi.org/10.1101/gr.239244.118.
[33] P. Geeleher, N. Cox, R.S. Huang, pRRophetic: an R package for prediction of clinical chemotherapeutic response from tumor gene expression levels, PLoS One 9 (9) (2014), e107468, https://doi.org/10.1371/journal.pone.0107468.
[34] K. Yoshihara, et al., Inferring tumour purity and stromal and immune cell admixture from expression data, Nat. Commun. 4 (2013) 2612, https://doi.org/10.1038/ncomms3612.
[35] S. Zuo, et al., Pan-cancer analysis of immune cell infiltration identifies a prognostic immune-cell characteristic score (ICCS) in lung adenocarcinoma, Front. Immunol. 11 (2020) 1218, https://doi.org/10.3389/fimmu.2020.01218.
[36] J. Sun, et al., Identification of tumor immune infiltration-associated lncRNAs for improving prognosis and immunotherapy response of patients with non-small cell lung cancer, Journal for immunotherapy of cancer 8 (1) (2020), e000110, https://doi.org/10.1136/jitc-2019-000110.
[37] M. Binnewies, et al., Understanding the tumor immune microenvironment (TIME) for effective therapy, Nat. Med. 24 (5) (2018) 541–550, https://doi.org/10.1038/s41591-018-0014-x.
[38] S. Valpione, et al., The T cell receptor repertoire of tumor infiltrating T cells is predictive and prognostic for cancer survival, Nat. Commun. 12 (1) (2021) 4098, https://doi.org/10.1038/s41467-021-24343-x.
[39] W.H. Fridman, et al., The immune contexture in human tumours: impact on clinical outcome, Nat. Rev. Cancer 12 (4) (2012) 298–306, https://doi.org/10.1038/nrc3245.
[40] B. Farhood, M. Najafi, K. Mortezaee, CD8+ cytotoxic T lymphocytes in cancer immunotherapy: a review, J. Cell. Physiol. 234 (6) (2019) 8509–8521, https://doi.org/10.1002/jcp.27782.
[41] A. Sarvaria, J.A. Madrigal, A. Saudemont, B cell regulation in cancer and anti-tumor immunity, Cell. Mol. Immunol. 14 (8) (2017) 662–674, https://doi.org/10.1038/cmi.2017.35.
[42] C. Groth, et al., Immunosuppression mediated by myeloid-derived suppressor cells (MDSCs) during tumour progression, Br. J. Cancer 120 (1) (2019) 16–25, https://doi.org/10.1038/s41416-018-0333-1.
[43] X. Jiang, et al., Role of the tumor microenvironment in PD-L1/PD-1-mediated tumor immune escape, Mol. Cancer 18 (1) (2019) 10, https://doi.org/10.1186/s12943-018-0928-4.
[44] J.N. Bodor, Y. Boumber, H. Borghaei, Biomarkers for immune checkpoint inhibition in non-small cell lung cancer (NSCLC), Cancer 126 (2) (2020) 260–270, https://doi.org/10.1002/cncr.32468.
[45] L. Liu, et al., Efficacy and safety of first-line immunotherapy combinations for advanced NSCLC: a systematic review and network meta-analysis, J. Thorac. Oncol. 16 (7) (2021) 1099–1117, https://doi.org/10.1016/j.jtho.2021.03.016.
[46] T.S.K. Mok, et al., Pembrolizumab versus chemotherapy for previously untreated, PD-L1-expressing, locally advanced or metastatic non-small-cell lung cancer (KEYNOTE-042): a randomised, open-label, controlled, phase 3 trial, Lancet 393 (10183) (2019) 1819–1830, https://doi.org/10.1016/S0140-6736(18)32409-7.
[47] M. Boyer, et al., Pembrolizumab plus ipilimumab or placebo for metastatic non-small-cell lung cancer with PD-L1 tumor proportion score $\geq$ 50%: randomized, double-blind phase III KEYNOTE-598 study, J. Clin. Oncol. 39 (21) (2021) 2327–2338, https://doi.org/10.1200/jco.20.03579.
[48] M. Reck, et al., First-line nivolumab plus ipilimumab with two cycles of chemotherapy versus chemotherapy alone (four cycles) in advanced non-small-cell lung cancer: CheckMate 9LA 2-year update, ESMO open 6 (5) (2021), 100273, https://doi.org/10.1016/j.esmoop.2021.100273.
[49] M. Yarchoan, et al., PD-L1 expression and tumor mutational burden are independent biomarkers in most cancers, JCI Insight 4 (6) (2019), https://doi.org/10.1172/jci.insight.126908.
[50] R.M. Samstein, et al., Tumor mutational load predicts survival after immunotherapy across multiple cancer types, Nat. Genet. 51 (2) (2019) 202–206, https://doi.org/10.1038/s41588-018-0312-8.
[51] Z. Zou, et al., Identification of tumor-infiltrating immune cells and microenvironment-relevant genes in nasopharyngeal carcinoma based on gene expression profiling, Life Sci. 263 (2020), 118620, https://doi.org/10.1016/j.lfs.2020.118620.
[52] J. Julamanee, et al., Composite CD79A/CD40 co-stimulatory endodomain enhances CD19CAR-T cell proliferation and survival, Mol. Ther. 29 (9) (2021) 2677–2690, https://doi.org/10.1016/j.ymthe.2021.04.038.
[53] G. Zhu, et al., Expression and role of dickkopf-1 (Dkk1) in tumors: from the cells to the patients, Cancer Manag. Res. 13 (2021) 659–675, https://doi.org/10.2147/CMAR.S275172.
[54] J. Qian, et al., Dickkopf-1 (DKK1) is a widely expressed and potent tumor-associated antigen in multiple myeloma, Blood 110 (5) (2007) 1587–1594, https://doi.org/10.1182/blood-2007-03-082529.
[55] S. Gao, Y. Jin, H. Zhang, Pan-cancer analyses reveal oncogenic and immunological role of dickkopf-1 (DKK1), Front. Genet. 12 (2021), 757897, https://doi.org/10.3389/fgene.2021.757897.
[56] J. Zhang, et al., DKK1 promotes migration and invasion of non-small cell lung cancer via beta-catenin signaling pathway, Tumour Biol 39 (7) (2017), 1010428317703820, https://doi.org/10.1177/1010428317703820.
[57] J. Niu, et al., DKK1 inhibits breast cancer cell migration and invasion through suppression of β-catenin/MMP7 signaling pathway, Cancer Cell Int. 19 (2019) 168, https://doi.org/10.1186/s12935-019-0883-1.
[58] P. Zhan, et al., Prognostic value of vascular endothelial growth factor expression in patients with lung cancer: a systematic review with meta-analysis, J. Thorac. Oncol. 4 (9) (2009) 1094–1103, https://doi.org/10.1097/JTO.0b013e3181a97e31.
[59] C.A. Wang, S.J. Tsai, The non-canonical role of vascular endothelial growth factor-C axis in cancer progression, Exp. Biol. Med. 240 (6) (2015) 718–724, https://doi.org/10.1177/1535370215583802.
[60] E. Carrillo de Santa Pau, et al., Prognostic significance of the expression of vascular endothelial growth factors A, B, C, and D and their receptors R1, R2, and R3 in patients with nonsmall cell lung cancer, Cancer 115 (8) (2009) 1701–1712, https://doi.org/10.1002/cncr.24193.